This manuscript was accepted by J. Appl. Phys. Click here to see the version of record.

Multilayer phosphorene quantum dots in an electric field: energy levels and optical absorption

H. Abdelsalam,[1,*] V. A. Saroka,[2,†] I. Lukyanchuk,[3,4] and M. E. Portnoi[5,6]

[1] *Department of Theoretical Physics, National Research Center, Cairo,12622, Egypt*
[2] *Institute for Nuclear Problems, Belarusian State University, Bobruiskaya 11, 220030 Minsk, Belarus*
[3] *University of Picardie, Laboratory of Condensed Matter Physics, Amiens, 80039, France*
[4] *L. D. Landau Institute for Theoretical Physics, Moscow, Russia*
[5] *School of Physics, University of Exeter, Stocker Road, Exeter EX4 4QL, United Kingdom*
[6] *ITMO University, St. Petersburg 197101, Russia*

(Dated: September 1, 2018)

Triangular and hexagonal multilayer phosphorene quantum dots with armchair and zigzag terminations are investigated with the orthogonal tight-binding model. The effect of increasing the number of layers is revealed. The obtained results show that in a small size multilayer quantum dot the edge states are as sensitive to the out-of-plane external electric fields as the edge states in a single layer dot to the in-plane external electric fields. The investigated optical absorption cross sections show that armchair phosphorene quantum dots have a regular behavior which should be useful for infrared detectors. In particular, it was found that in hexagonal armchair phosphorene dots absorption peaks can be increased, decreased, or totally removed from the low-energy region depending on the orientation of the applied electric field. The effect of spurious doping can suppress the transitions < 0.4 eV, while effect of the finite temperature is almost negligible.

I. INTRODUCTION

Similar to other pnictogens (arsenic, antimony, bismuth and possibly moscovium) phosphorous is prone to form three bonds, which allows for the formation of its layered allotrope – black phosphorous. Recently, few-layer black phosphorous flakes have been isolated by both mechanical [1–3] and liquid exfoliation [4, 5]. These micrometer-size flakes have been shown to be highly conductive as compared to other 2D materials [1–3, 6–11]. Moreover, being a direct band gap semiconductor with a band gap dependent on the number of layers [12–15] they have optical responses that are sensitive to the stacking and number of layers [16–18].

The nanometer size flakes of a single- and few-layer black phosphorous are dubbed phosphorene quantum dots (PQDs). They have different properties as compared to micrometer size flakes. It is predicted that the edge states play a considerable role in PQDs electronic and optical properties. For example, PQDs can be conducting, semiconducting, or insulating depending on the applied electric and magnetic fields, shape and edge termination of the quantum dots [14, 19–22]. Recently it was shown that electron pair repulsion in black phosphorus (PB) is responsible for the peculiar edge effects and can be used in the damage-free surface functionalization of PB [23]. Moreover edge mixing, such as a triangular PQDs with both zigzag and armchair edges, provides a significant effect on the distribution and number of edge states [24]. Unlike single layer PQDs, the multilayer PQDs can be readily fabricated by liquid exfoliation [25–27]. The unique nonlinear absorption of the as-synthesized PQDs have been demonstrated to be promising in ultrafast photonics applications [28]. The tunable band gap and effective hole mobility higher than in other hole transport materials for perovskite solar cells make such PQDs of about 5 nm-size especially suitable for photovoltaic applications [29–31]. However, few theoretical investigations have been carried out for multilayer PQDs. For instance, only bilayer phosphorene quantum dots of rectangular shape subjected to perpendicular magnetic and electric fields have been studied [32].

In this paper, the electronic and optical properties of triangular and hexagonal multilayer PQDs are investigated under the effect of electric field. The present study is conducted for zigzag and armchair terminations and ABA stacking order. All three directions (in plane x and y and out-of-plane z) are considered for the application of the electric field in order to find the most efficient way of tuning multilayer PQDs electronic and optical properties. The results presented hereafter could be verified by the spatial modulation spectroscopy technique which is a state-of-the-art tool for direct measurements of individual nanoobjects absorption spectra [33–35].

II. THEORETICAL MODEL

The electronic properties of phosphorene clusters subjected to an electric field can be calculated using the tight-binding Hamiltonian:

$$H = \sum_{\langle ij \rangle} t_{ij} c_i^\dagger c_j + \sum_i V_i(E)\, c_i^\dagger c_i, \qquad (1)$$

where $c_i^\dagger$ and c_i are the electron creation and annihilation operators t_{ij} is the hopping integral between i-th

* hazem.abdelsalam@etu.u-picardie.fr
† 40.ovasil@gmail.com

and j-th atomic sites and V_i is the on-site electron energy that depends both on the local atomic environment and on the applied electric field. As has been recently shown by Rudenko et al. [13, 36], fifteen hopping parameters are needed for a realistic tight-binding description of the multilayer black phosphorus. We employ these parameters to model the electronic properties of multilayer phosphorene quantum dots [see Fig. 1]. For convenience,

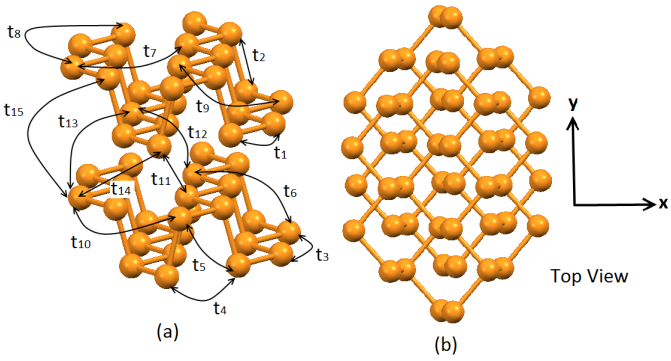

FIG. 1: (a) The geometrical structure and tight-binding hopping parameters t_{ij} of the phosphorene bilayer. (b) Top view of the bilayer PQD with $n_l = 48$ atoms.

the values of the hopping parameters from Ref. [36] are given in Table I together with the distances between the corresponding sites of the lattice.

TABLE I: The tight-binding, t_i, and structural, d_i, parameters adapted from Ref. [36] for phosphorene based quantum dots

i	t_i eV	d_i Å
1	−1.486	2.22
2	3.729	2.24
3	−0.252	3.31
4	−0.071	3.34
5	0.019	3.47
6	0.186	4.23
7	−0.063	4.37
8	0.101	5.18
9	−0.042	5.37
10	0.073	5.49
11	0.524	3.60
12	0.180	3.81
13	−0.123	5.05
14	−0.168	5.08
15	0.005	5.44

In order to study the optical properties of phosphorene quantum dots we calculate their optical absorption cross sections [20, 37, 38]:

$$\sigma(\varepsilon) \sim \sum_{i,f} [n(\varepsilon_i) - n(\varepsilon_f)]\, S(\varepsilon_{i,f}) \exp\left[-\frac{(\varepsilon - \varepsilon_{i,f})^2}{\alpha^2}\right] \quad (2)$$

where $S(\varepsilon_{i,f})$ is the oscillator strength. In Eq. (2) the Fermi-Dirac distribution function, $n(\varepsilon)$, has been introduced to account for temperature and Fermi level position effects; also, the Gaussian-type exponent is used instead of Dirac delta function to incorporate absorption peak broadening, α, due to the finite lifetimes of excited carries. Throughout this paper the broadening $\alpha = 0.02$ eV is used.

III. RESULTS AND DISCUSSION

In what follows, for multilayer PQDs classification we use the approach proposed for single layer dots in Ref. [20]. Thus, the multilayer PQD is a cluster of atoms cut from a few-layer phosphorene sheet similar to what can be done for other 2D material based nanostructures [39–41]. The edges of the dots are assumed to be passivated by oxygen to prevent the possible edge reconstruction and disappearance of the edge states [42]. Thereafter, we refer to the triangular and hexagonal quantum dots with zigzag terminations as ZTRI and ZHEX, respectively. Similarly, ATRI/AHEX refers to triangular/hexagonal QDs with armchair terminations. The number of atoms in one layer is denoted by n. In N-layer structure each layer contains the same amount of atoms, hence the total number of atoms $n_l = Nn$. For the model we study, we chose structures based on single layer ZTRI $n = 222$, ZHEX $n = 216$, ATRI $n = 216$, and AHEX $n = 222$ phosphorene quantum dots, with the lateral sizes, estimated as in Ref. [20], $L \approx 3.55$, 1.96, 3.3 and 1.85 nm, respectively. The vertical size of the dots $H = hN$, where $h \approx 0.55$ nm is the vertical shift between the neighbouring layers [1]. For typical 3-5-layer PQDs H ranges from 1.65 to 2.75 nm.

A. Energy levels: stacking and electric field effects

By applying out-of-plane, E_z, and in-plane, E_x and E_y, electric fields to the phosphorene dots with increasing number of layers the electric field and stacking effects on the energy levels can be revealed. Since SiO_2 is often used as a substrate for PQD samples preparation, the QD energy levels are investigated up to electric breakdown field of SiO_2 0.1 V/Å [43]. Such an upper limit of electric field is often used in theoretical studies of various nanostuctures [40, 44].

In order to unveil the pure effect of stacking, i.e. the increasing number of layers, on PQD energy levels, let us consider the left hand side of the plots in the Figs. 2 and 3 corresponding to zero external electric field. In all the plots one can clearly see a group of states distributed in a wide energy range around the Fermi level, which is set to $\varepsilon_F = 0$ eV. This distinctive group of states consists of the edge states [see Fig. 10 in Appendix A] originating from the quasi-zero energy states discussed in work [20]. Their number is given by N_{QZES} in Table

III of Ref. [20] for single layer structures and it must be multiplied by number of layers in multilayer ones. The specified group of edge states is separated from the lower/higher valence/conduction band states by the two mini energy gaps. **The overall band gap, containing the edge states and the two mini band gaps, in each cluster is shown in Figs. 2 - 4 by the region between the two red lines. The blue line in these figures represents the Fermi energy that can be clearly seen in Fig. 3 (b, d).** These minigaps close as the number of layers increases with an exception of AHEX quantum dots. For all other structures in question, the minigap above the Fermi level prone to close completely, whereas the minigap below the Fermi level approaches a threshold.

Having revealed the general trends in the stacking effect of PQDs, we proceed with an analysis of the energy level dependence on the external fields. For single layer PQDs under E_z field this value is small and the effect of electric field is negligible [see Fig. 2 (a)]. The effect of E_z on edge states start to appear on bilayer and increase by increasing the number of layers because the distance between the layers increases the potential energy, generated by the electric field, on the upper and lower sub-layer of the multilayer PQDs. The generated potential on the layered structure as a function of the layers separation and electric field is given by $V = \pm eER$, where $\pm$ stand for upper and lower sublayers, respectively, E is the electric field applied across the structure. For E_z electric field $R = H$ is the separation between the first and the last layers of the multilayer system. The observation of the electric field effect for single layer PQD in E_z-field requires high strength fields, which may not be experimentally available. To overcome this problem, the in-plane field can be applied along the x- and y-directions. In this case, $R = L$ is the PQD lateral size, which is much larger than the distance between the sublayers of a single layer PQD, therefore an efficient control of quantum dot energy levels should be possible for moderate external fields. Both above-mentioned cases will be considered in what follows.

Let us start form the effect of the perpendicular electric field. The energy levels of ZTRI and AHEX QDs subjected to the electric E_z-field are presented in Fig. 2. In multilayer ZTRI PQDs, the applied field decreases the energy gap between edge states and valence band states in bilayer and closes the gap completely in trilayer PQDs at $E_z = 0.08$ V/Å, as seen in Fig. 2 (e). The value at which the electric field closes this gap depends on the number of layers. The edge states in AHEX PQDs presented in Fig. 2 (b, d, f) show different behaviour. Upon application of the external E_z-field the group of the edge states energy levels splits onto subgroups corresponding to the number of sublayers in the system. The same is true for ATRI QDs with the only difference that edge states are more dispersed in the energy in ATRI dots than in AHEX. The electric field influence on the energy levels of ZHEX PQDs is similar to that for ZTRI dots,

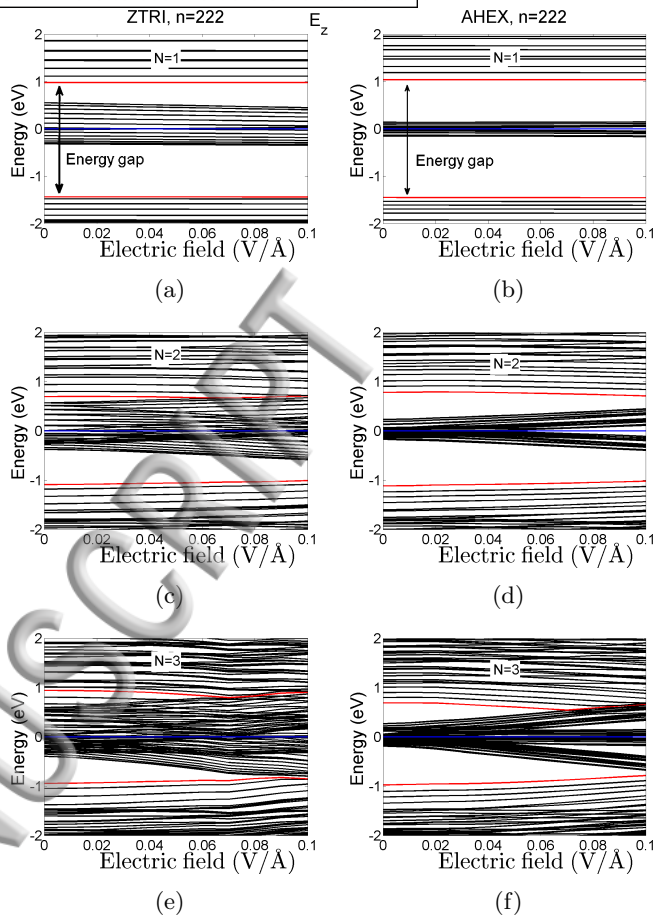

FIG. 2: Electronic energy levels as a function of perpendicular electric field for ZTRI (a, c, e) and for AHEX (b, d, f) with the total number of layers $N = 1$, 2, and 3. The red lines and the blue lines shown in this figure and the following figures are: The upper red line represent the lowest unoccupied energy level, the lower one is the highest occupied energy level, and the blue line is the Fermi level.

therefore we do not present results for ZHEX, as well as ATRI dots, subjected to E_z-field.

The effect of E_x-field on the edge states of multilayer PQDs is shown in Fig. 3 for ZTRI (a, c) and ZHEX (b, d) PQDs. As one can see, the in-plane E_x-field divides the edge states in multilayer ZTRI PQDs into two groups. One of them experiences a strong shift towards the conduction band states, whereas another group, containing the rest of edge states, stays almost stationary around the Fermi energy. It is worth noting that a similar behavior has been reported in single layer ZTRI PQDs under high perpendicular electric field in Ref. [20]. The number of edge states in each group is discussed in Ref. [20], for multilayer this number is multiplyed by N. For example, in ZTRI having even number of atoms, $n = 222$ and $N = 3$, there are three edge states in the group shifting towards the conduction band.

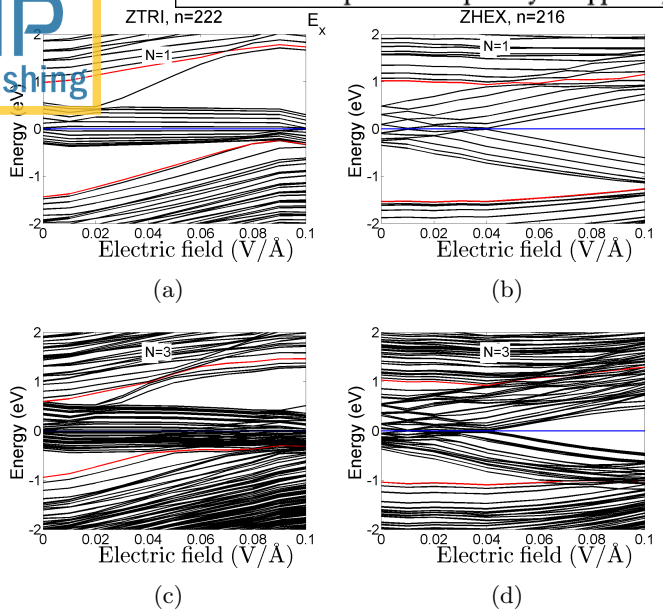

FIG. 3: The energy levels of (a, b) single and (c, d) trilayer PQDs subjected to the in-plane E_x-field: (a, c) ZTRI and (b, d) ZHEX.

The geometrical shape of ZHEX provides an equal number of edge states in the upper and the lower sublayers of PQDs. Therefore, in Fig. 3 (b, d) the applied in-plane E_x-field split the edge states into two equal groups: one shifting towards conduction band states and another shifting towards valence band states – whereby ZHEX quantum dots experience a "metal-semiconductor" transition. Anticrossings between edge states [22] are also observed inside each group and between the two groups.

For ZTRI quantum dots all the edge atoms have the same x-coordinate. This prevents tunability of the edge states by applying the in-plane E_x-field. However, since these edge atoms have different y-coordinates, the splitting of the edge states energy levels is possible due to different on-site energies generated by E_y-field. Figure 4 (a, c) shows high efficiency of the edge states manipulation in ZTRI PQDs by E_y-field as compared to that for E_x-field. For ZHEX structure the picture is qualitatively different. Nonetheless, it can be interpreted in a similar manner. The edge atoms of the dot can be divided into pairs having the the same y-coordinates, therefore, applying the E_y-field, we see the doubly degenerate energy levels in Fig. 4 (b, d). The E_y-field cannot lift the degeneracy of these levels. However, for each pair the x-coordinates of the atoms forming the pair are different, therefore the levels can be split by applying E_x-field. In general, such pairing is also happening for ATRI and AHEX structures. As a result, we see that the edge states energy levels as functions of the E_y-electric field form something like rays. These rays are especially well seen for monolayer ZHEX and AHEX quantum dots. The number of the rays is equal to the half of the number of the edges states. For multilayer dots each ray contains a bunch of curves but the number of rays is the same as for the corresponding monolayer dot. The presented diversity of the energy levels behaviour in external electric fields is important for multilayer PQDs optical properties presented next. **It is worth noting that the total number of atoms (n) used in our investigations is arbitrary and the obtained results are applicable to other structures characterized by greater or lesser value of n. For example, as seen in Fig. 12 in appendix B, the effect of electric field on PQDs ZTRI with $n = 141$ and ZHEX with $n = 150$, is qualitatively the same as in Fig. 4.**

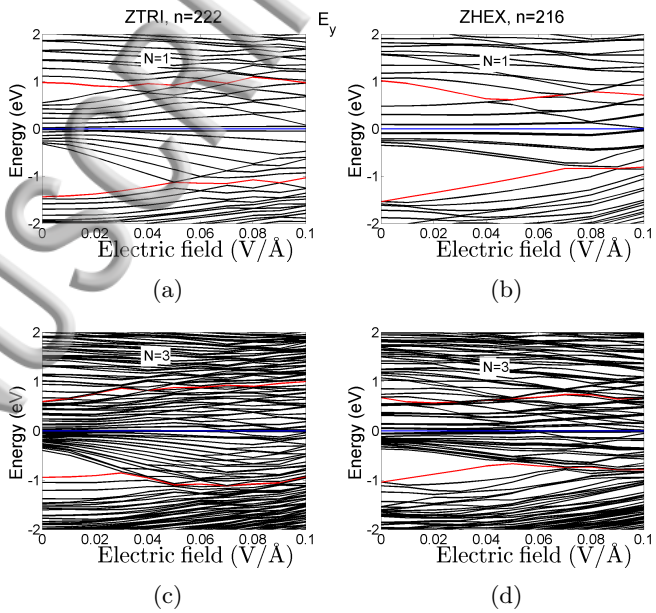

FIG. 4: The energy levels of (a, b) single and (c, d) trilayer ZTRI and ZHEX PQDs subjected to the in-plane E_y-field.

B. Optical absorption cross section

Let us first consider multilayer PQD absorption due to dipole transitions without applied external fields. Fig. 5 shows the optical absorption cross section, σ, of single and multilayer ZTRI and ATRI PQDs. The optical cross sections, σ_x, σ_y, and σ_z, are normalized with respect to the maximum value of σ_y. Three colours correspond to the absorption cross sections for three polarizations of the incident light: green for σ_x, red for σ_y, and black for σ_z. As seen from Fig. 5 (a, c, e), the transitions between edge states for ZTRI are only due to the y-polarized incident electromagnetic wave (see σ_y). The higher energy transitions, i.e. the valence band states to edge states, edge states to conduction band states, and valence to conduction band states, are predominantly induced by the x-polarized waves (see σ_x). It is also seen in Fig. 5

(a, c, e) that at energies above 0.5 eV the contributions from σ_y and σ_z cross sections are minute. Although the total number of atoms in layered ZTRI and ATRI PQDs is nearly the same, the low-energy spectra of ATRI for all three polarizations are richer with absorption peaks. This is clearly seen in Fig. 5 (b). The rich absorption peak structure in multilayer ATRI PQDs results from the spreading of edge states in the energy gap between conduction and valence band states (see Fig. 11 in Appendix B). By increasing the number of layers the number of edge states increases in the energy gap making ATRI PQDs a wide band mid- and far-infrared absorber. Another difference between ZTRI and ATRI PQDs is the presence of intense σ_y absorption peaks (as compared to σ_x ones) in the region 2–3 eV for multilayer ATRI quantum dots. Besides, for double and trilayer ATRI dots the σ_z-absorption for $\varepsilon < 0.3$ eV is comparable to those of σ_x and σ_y. This is clearly seen in Fig. 5 (d) and (f), respectively. The absorption spectra of single and multilayer ZHEX and AHEX PQDs exhibit behavior similar to those of ZTRI and ATRI spectra, respectively (see Fig. 13 in Appendix C). In conclusion, due to the higher number of edge states, the armchair phosphorene quantum dots of both triangular and hexagonal shapes should be preferable in infrared detectors than the corresponding zigzag dots.

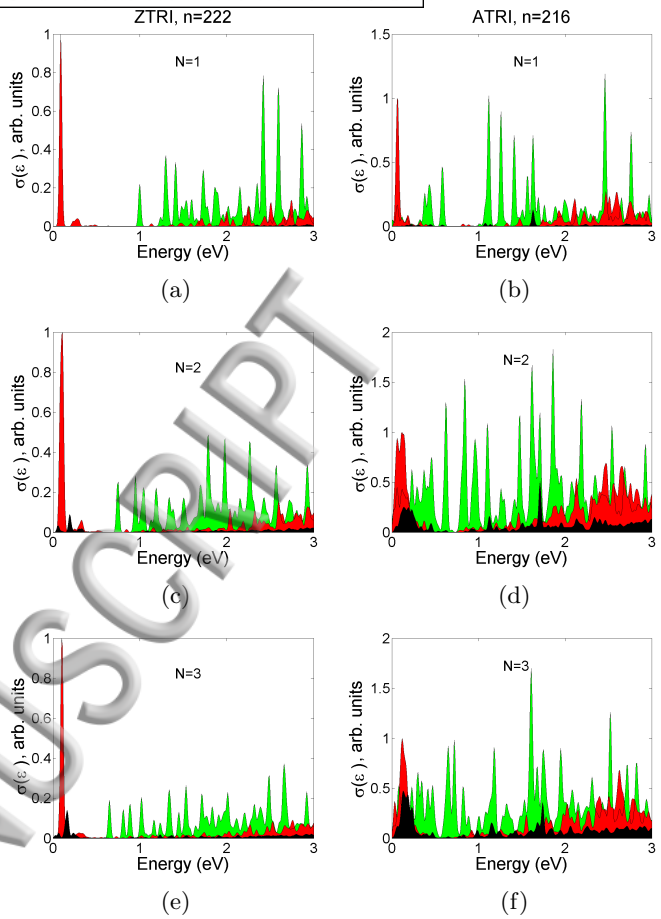

FIG. 5: Optical absorption cross section for multilayer ZTRI and ATRI PQDs.Three colours (online only) represent the three absorption cross sections, green for σ_x, red for σ_y, and black for σ_z.

C. Electric field effect on the optical absorption spectrum

In this section, we proceed with optical properties of multilayer phosphorene QDs in the external electric field. For presentation purposes, we choose trilayer PQDs, which their energy levels behaviour in various electric fields is shown in Figs. 2, 3, 4, and 11. The optical absorption cross section of ZTRI trilayer PQDs subjected to electric field directed along z- and x-axis are presented in Fig. 6 for three values of the applied field: 0.02, 0.06, and 0.1 V/Å. It can be noticed that due to $E_z = 0.02$ V/Å the absorption peaks in the energy region $\varepsilon < 2$ eV homogenize to a relatively flat spectrum. The absorption cross sections at $\varepsilon > 2$ eV in Fig. 6 (a) are very similar to those in Fig. 5 (e) at $E_z = 0$ V/Å. This is in agreement with the small splitting of the energy levels seen in Fig. 2 (e) at $E_z = 0.02$ V/Å. Another noticeable feature of the trilayer ZTRI PQD absorption spectrum is a significant blue shift of about 0.3 eV for the σ_z-low energy absorption shown by the group of black peaks at $\varepsilon = 0.4$ eV in Fig. 6 (c). One can also notice that the intensity of σ_x- and σ_y-absorption at $\varepsilon > 1$ eV increases with applied E_z-field with respect to the low-energy σ_y-peak used as a reference. The latter contrasts with the σ_x and σ_y-absorption behaviour in the E_x-field shown in Fig. 6 (b, d, f). One can point out a considerable increase of σ_x- and σ_z-absorption intensities around $\varepsilon = 0.4$ eV as the field attain $E_x = 0.1$ V/Å. At the same time, the most intense σ_y peak (red), which results from transitions between the edge states, is almost unaffected by the electric field neither E_x nor E_z.

For the sake of completeness, we present in Fig. 7 the optical absorption cross sections of AHEX triangular PQDs placed into E_z and E_x fields. This figure shows that the two fields act very differently on the same multilayer AHEX PQD. In particular, E_x-field opens an optical absorption gap, while E_z-field closes it. This optical gap seen in Fig. 7 (d, f) is consequence of the energy gap opened between the edge states by E_x-field as shown in Fig. 11 (d). Thus, we have shown that a proper choice of the electric field and the multilayer phosphorene quantum dot shape provide a versatile control over its optical properties.

D. Fermi level and temperature dependence

In sections III B and III C, the optical absorption is presented for zero temperature and intrinsic position of the Fermi level. The absorption measurements, how-

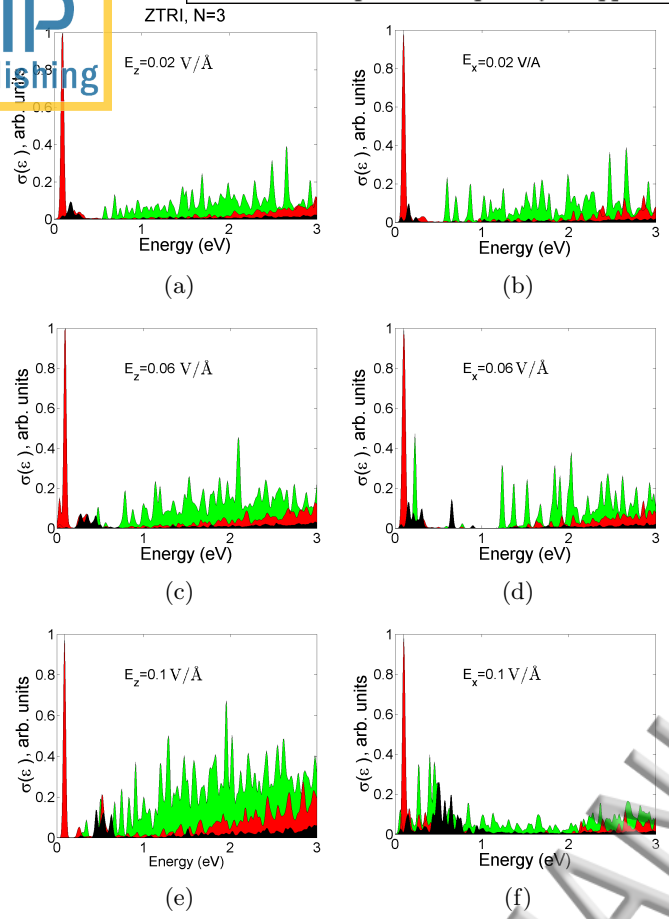

FIG. 6: The absorption cross section of trilayer ZTRI PQDs subjected to (a, c, e) perpendicular, E_z, and (b, d, f) in-plane, E_x, electric fields. Similar to Fig. 5 the green, red, black peaks represent σ_x, σ_y, and σ_z absorption cross sections, respectively.

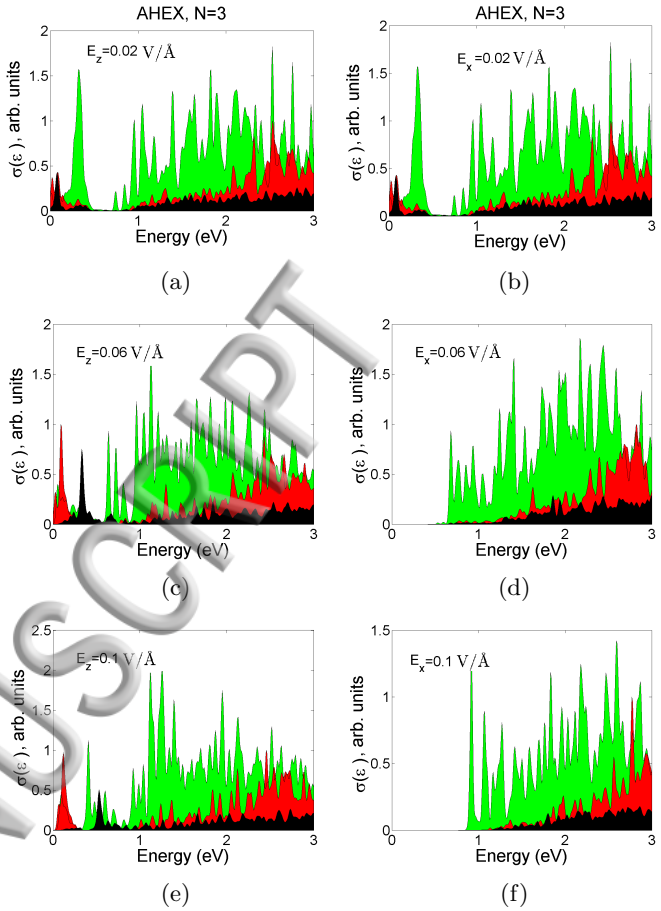

FIG. 7: The same as Fig. 6 but for trilayer AHEX PQDs.

ever, are always carried out at finite temperature. The Fermi level of individual quantum dots in measured samples may also be affected by chemicals such as N-methylpyrrolidone [25], isopropyl or ethyl alcohol [45] used in the liquid exfoliation of phosphorene. The two mentioned aspects can modify low-energy absorption involving transitions with the edge states. Figure 8 reveals the effect of the Fermi level position and finite temperature for multilayer PQDs. Since this effect should be the strongest in PQDs with densely packed edges states, the trilayer ATRI and AHEX quantum dots have been chosen for investigation [see Fig. 11 in Appendix B]. As follows from Fig. 8 (a, b) the Fermi level position drastically modifies low-energy absorption for all three polarizations of the incident light. The most profound changes are observed for the absorption below 0.4 eV. It should be noted that increasing the Fermi level leads not only to variation of the intensity of the absorption peaks [see panels for σ_x in Fig. 8 (a, b)] but also to the peak splitting and absorption red shift [see panels for σ_y in Fig. 8 (a, b)]. In contrast, the influence of the temperature on PQDs absorption is less profound even at $T = 400$ K. As one can see, in Fig. 8 (c, d), for both chosen trilayer PQDs the absorption variations are moderate even for photon energies < 0.4 eV.

If an individual quantum dot is supplied with contacts, the E_z-field applied via back gate voltage vary the quantum dot Fermi level. According to the results presented in Fig. 8, such electrostatic doping can be used to modify intensity of the low-energy absorption peaks of PQDs in a controlled manner similar to what has been proposed for graphene nanoribbons with edge states [46–48].

E. Joint density of states and the forbidden optical transitions

According to the presented results, the absorption spectra of armchair flakes have a considerably higher number of absorption peaks than in zigzag flakes. In order to explain this effect we plot the joint density of states (JDOS). This quantity, if considered in conjunction with the total absorption cross-section ($\sigma_x + \sigma_y$

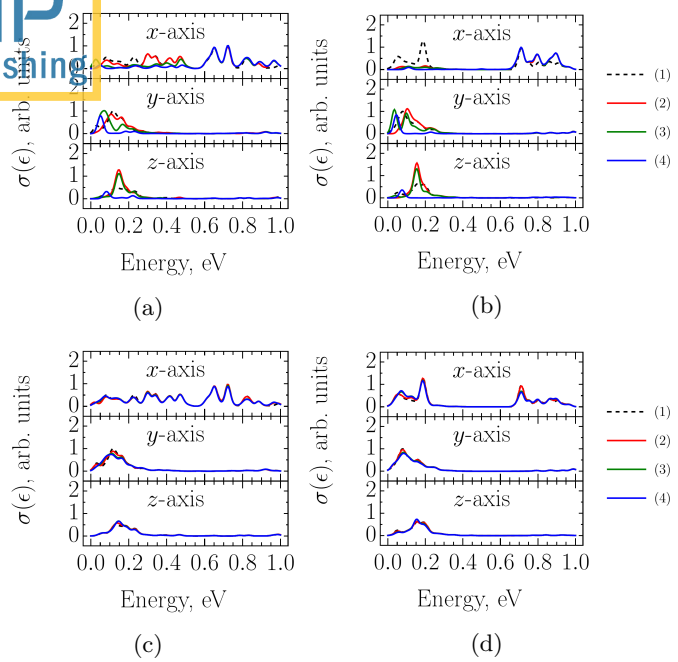

FIG. 8: The optical absorption of trilayer (a, c) ATRI and (b, d) AHEX PQDs for various positions of the Fermi level (a, b): (1) $\varepsilon_F = 0$, (2) 0.06, (3) 0.12 and (4) 0.24 eV; and various temperatures (c, d): : (1) $T = 0$, (2) 77, (3) 300 and (4) 400 K.

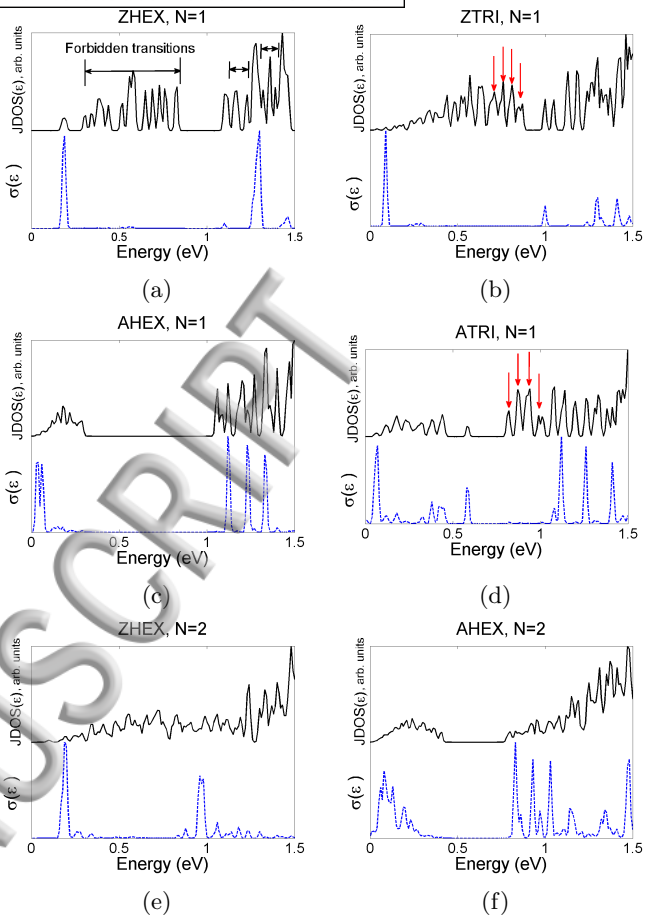

FIG. 9: The joint density of states and the corresponding optical absorption spectrum for hexagonal and triangular phosphorene single layer (a, b, c, d) and bilayer (e, f) quantum dots.

$+ \sigma_z$), unveils the allowed and forbidden transitions in the selected quantum dots [49]. These calculations are performed for hexagonal and triangular dots with zigzag and armchair terminations. Fig. 9 illustrates the JDOS and the corresponding optical absorption cross-section for single (Fig. 9 a, b, c, d) and bilayer (Fig. 9 e, f) quantum dots. It is clearly seen that the number of forbidden transitions in ZHEX and ZTRI are higher than that in AHEX or ATRI ones. For instance, in ZHEX quantum dots, transitions in the energy range from 0.3 to 1.25 eV as in Fig. 9 (a) are not allowed, therefore they are missing in the absorption spectrum.

These dipole transitions are due to transitions between edge states and the lowest unoccupied energy states. The same transitions exist in ZTRI and are forbidding transitions also (See Fig. 9 (b)). In case of AHEX or ATRI the number of forbidden transitions is lower than in zigzag flakes, almost all the transitions between edge states is allowed in armchair flakes. This is seen by comparing the forbidden transitions in ZTRI (Fig. 9 (b)) and ATRI (Fig. 9 (d)) PQDs. However, the number of forbidden transitions between edge states and the lowest unoccupied energy states are approximately equal to those in zigzag PQDs: see the peaks marked with the red arrows in Fig. 9 (b) and (c).

IV. CONCLUSIONS

In conclusion, we have investigated the electronic and optical properties of multilayer phosphorene quantum dots of triangular and hexagonal shapes with zigzag and armchair edge terminations. It has been found that increasing the number of layers increases the number of edge states in the low-energy region around the Fermi level as well as closes the energy minigaps between the edge states and valence/conduction band states. Only in armchair phosphorene quantum dots, the dispersion of the edge states around the Fermi level is narrow enough to prevent complete closing of the minigaps at least up to five layers. However, these gaps of armchair quantum dots can be closed by applying external E_x-, and E_z-electric fields. It has been also found that in AHEX dots the E_z-field split the edges state group onto subgroups equal to the number of sublayers in the dot, while E_x-field divides edge states into two subgroups independently of the number of layers. The latter is observed for all the types of multilayer PQDs except for the ZTRI

dots.

If follows from our results that the behavior of the edge states of PQDs in external electric field is predominantly demned by potentials generated on the edge atoms, where the electron density is localized. It should be noted that this potentials can be also affected by the chemical functionalization of the dots, therefore our results provide a road map for efficient chemical functionalization of such structures. Attaching different chemical groups to the edge atoms of PQDs, as it has been done for graphene quantum dots [50, 51], one can induce potential difference, i.e. dipole moment, giving rise to the intrinsic electric field within the dots.

For optical absorption cross sections it has been found that quantum dots with armchair edges should be more preferable for polarization sensitive infrared detectors. For visible frequency range (from 2 to 3 eV) the anisotropy of the armchair PQDs absorption between x- and y-polarizations drops down as compared to infrared region. The E_x-field applied to armchair PQDs totally remove that peaks from the low-energy region opening an optical energy gap up to 0.8 eV. In contrast, in ZTRI PQDs the same field significantly increases intensity of absorption in this region.It should be also noted that the low-energy absorption peaks, < 0.4 eV, may be completely suppressed by spurious doping of the individual dots, while the effect of temperature is less essential. An additional modification of the optical absorption spectrum that is beyond the scope of this paper may arise due to the interaction between the substrate and the quantum dots. The dielectric confinement may also has a considerable effect on the exciton binding energy and the excitonic spectrum [52]. However, since we are targeting the intrinsic properties of the dot, such as shape, edge termination, and number of layer, we assume the usage of the substrates that weakly interact with the PQDs such as h-BN [53] and we chose quantum dots with a relatively small lateral size that is less than the exciton Bohr radius (3-4 nm, [54]) to minimize excitonic effects.

ACKNOWLEDGMENTS

This work was supported by the EU FP7 ITN NOTEDEV (FP7-607521), EU H2020 RISE project CoExAN (H2020-644076), and FP7 IRSES projects CANTOR (FP7-612285). The work of MEP was financially supported by the Government of the Russian Federation through the ITMO Fellowship and Professorship Program. The authors are very grateful to C. A. Downing for the careful reading of the manuscript.

Appendix A: Edge states in multilayer PQDs

In this appendix section, we demonstrate that the peculiar group of the energy states in the bulk energy gap of multilayer PQD contains the so-called edge states, with their electron density distribution localized at the edges of the quantum dot. In Fig. 10 this is clearly shown for the two chosen states of a trilayer AHEX PQD. The overlapping between the electron charge densities is also seen.

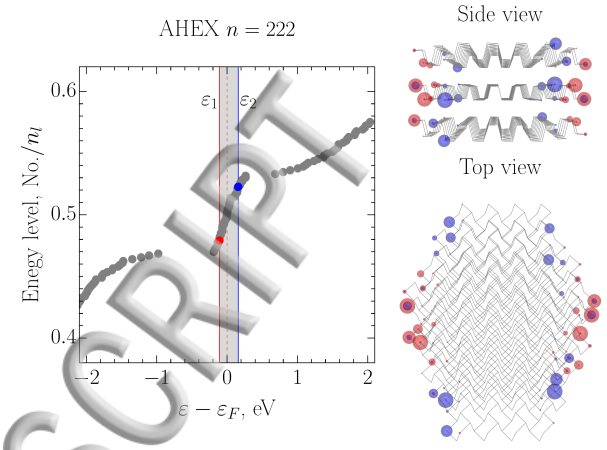

FIG. 10: The energy levels of trilayer AHEX PQD with electron density distribution shown for the selected edge states.

Appendix B: Multilayer PQDs energy levels in electric fields

In Fig. 11 the electronic states of ATRI and AHEX multilayers PQDs are presented as a function of electric E_x-field. Similar to ZHEX PQDs the edge states in AHEX split open the energy gap between the edge states. In ATRI dots the energy levels behaviour is qualitatively the same but with smaller corresponding energy gaps. For both PQD types presented in Fig. 11 the minigaps between edge states and bulk states decrease as N changes from (a, b) 1 to (e, f) 5-layers.

In order to confirm the generality of the obtained results for different values of the total number of atoms (n). We consider in Fig. 12 the effect of in-plane electric field directed in y-direction (E_y) on the energy levels of ZTRI and ZHEX having $n = 141$ and $n = 150$, respectively. As shown by Fig. 12, the behavior of the energy levels under the effect of E_y field is qualitatively similar to that in Fig. 4.

Appendix C: Optical absorption

Herein, Fig. 13, we provide optical absorption calculations for layered ZHEX and AHEX PQDs, which in addition to optical absorption of ATRI confirm the rich optical transitions in multilayer PQDs with armchair terminations.

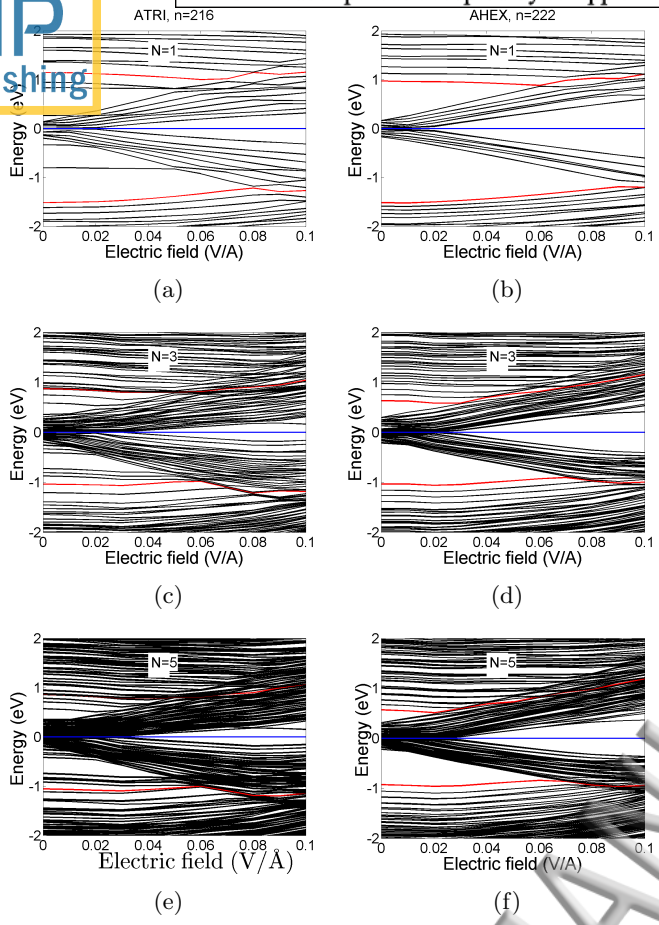

FIG. 11: The energy levels as a function of electric E_x-field for (a, c, e) ATRI and (b, d, f) AHEX PQDs.

[1] A. Castellanos-Gomez, L. Vicarelli, E. Prada, J. O. Island, K. L. Narasimha-Acharya, S. I. Blanter, D. J. Groenendijk, M. Buscema, G. A. Steele, J. V. Alvarez, H. W. Zandbergen, J. J. Palacios, and H. S. J. van der Zant, 2D Mater. **1**, 025001 (2014).

[2] L. Li, Y. Yu, G. J. Ye, Q. Ge, X. Ou, H. Wu, D. Feng, X. H. Chen, and Y. Zhang, Nat. Nanotechnol. **9**, 372 (2014).

[3] H. Liu, A. T. Neal, Z. Zhu, Z. Luo, X. Xu, D. Tománek, and P. D. Ye, ACS Nano **8**, 4033 (2014).

[4] J. R. Brent, N. Savjani, E. A. Lewis, S. J. Haigh, D. J. Lewis, and P. O'Brien, Chem. Commun. **50**, 13338 (2014).

[5] P. Yasaei, B. Kumar, T. Foroozan, C. Wang, M. Asadi, D. Tuschel, J. E. Indacochea, R. F. Klie, and A. Salehi-Khojin, Adv. Mater. **27**, 1887 (2015).

[6] J. Qiao, X. Kong, Z.-X. Hu, F. Yang, and W. Ji, Nat. Commun. **5**, 4475 (2014).

[7] A. N. Rudenko and M. I. Katsnelson, Phys. Rev. B **89**, 201408 (2014).

[8] K. Dolui and S. Y. Quek, Sci. Rep. **5**, 11699 (2015).

[9] Z. Sun, H. Xie, S. Tang, X.-F. Yu, Z. Guo, J. Shao, H. Zhang, H. Huang, H. Wang, and P. K. Chu, Angew. Chemie Int. Ed. **54**, 11526 (2015).

[10] Z. T. Jiang, Z. T. Lv, and X. D. Zhang, Phys. Rev. B **94**, 115118 (2016).

[11] J.-Y. Wu, S.-C. Chen, G. Gumbs, and M.-F. Lin, Phys. Rev. B **95**, 115411 (2017).

[12] J. Dai and X. C. Zeng, J. Phys. Chem. Lett. **5**, 1289 (2014).

[13] A. N. Rudenko, S. Yuan, and M. I. Katsnelson, Phys. Rev. B **92**, 085419 (2015).

[14] Z. T. Jiang, S. Li, Z. T. Lv, and X. D. Zhang, AIP Adv. **7**, 045122 (2017).

[15] D. J. P. de Sousa, L. V. de Castro, D. R. da Costa, J. M. Pereira, and T. Low, Phys. Rev. B **96**, 155427 (2017).

[16] T. Low, A. S. Rodin, A. Carvalho, Y. Jiang, H. Wang, F. Xia, and A. H. Castro Neto, Phys. Rev. B **90**, 075434 (2014).

[17] D. Çakir, C. Sevik, and F. M. Peeters, Phys. Rev. B **92**, 165406 (2015).

[18] L. Li, J. Kim, C. Jin, G. J. Ye, D. Y. Qiu, F. H. da Jornada, Z. Shi, L. Chen, Z. Zhang, F. Yang, K. Watanabe, T. Taniguchi, W. Ren, S. G. Louie, X. H. Chen, Y. Zhang, and F. Wang, Nat. Nanotechnol. **12**, 21 (2016).

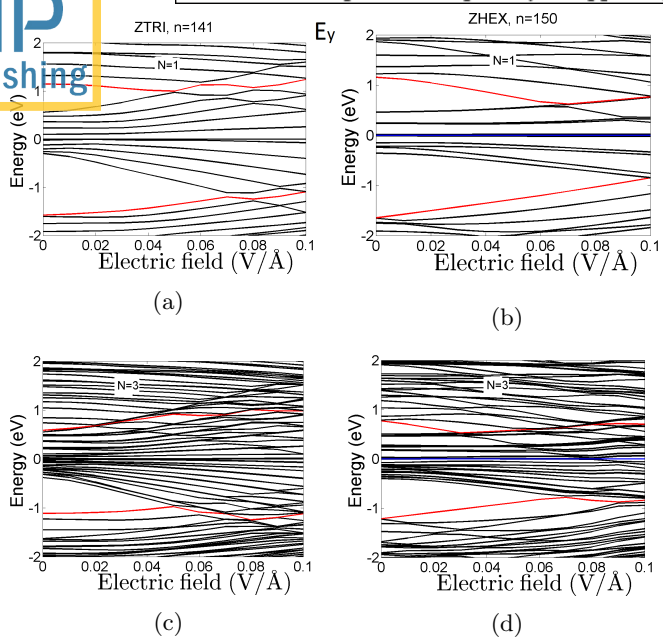

FIG. 12: The energy levels of single layer (a, b) and trilayer (c, d) ZTRI and ZHEX PQDs under the effect of the in-plane E_y-field for total number of atoms n=141 and n=150, respectively..

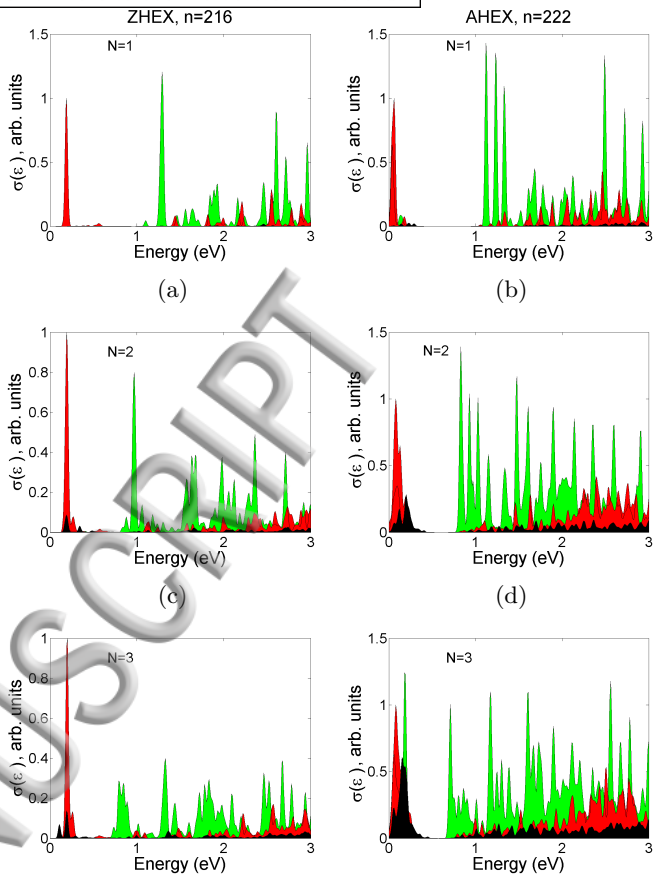

FIG. 13: The optical absorption cross section for (a, c, e) ZHEX and (b, d, f) AHEX N-layer PQDs.

[19] R. Zhang, X. Y. Zhou, D. Zhang, W. K. Lou, F. Zhai, and K. Chang, 2D Mater. **2**, 045012 (2015).

[20] V. A. Saroka, I. Lukyanchuk, M. E. Portnoi, and H. Abdelsalam, Phys. Rev. B **96**, 085436 (2017).

[21] J. S. de Sousa, M. A. Lino, D. R. da Costa, A. Chaves, J. M. Pereira, and G. A. Farias, Phys. Rev. B **96**, 035122 (2017).

[22] L. L. Li, D. Moldovan, W. Xu, and F. M. Peeters, Nanotechnology **28**, 085702 (2017).

[23] X.-P. Kong, X. Shen, and X. Gao, J. Phys. Chem. Lett. **9**, 947953 (2018).

[24] F. X. Liang, Y. H. Ren, X. D. Zhang, and Z. T. Jiang, J. Appl. Phys. **123**, 125109 (2018).

[25] X. Zhang, H. Xie, Z. Liu, C. Tan, Z. Luo, H. Li, J. Lin, L. Sun, W. Chen, Z. Xu, L. Xie, W. Huang, and H. Zhang, Angew. Chemie Int. Ed. **54**, 3653 (2015).

[26] Y. Xu, Z. Wang, Z. Guo, H. Huang, Q. Xiao, H. Zhan, and X.-F. Yu, Adv. Optical Mater. **4** (2017).

[27] J. Du, M. Zhang, Z. Guo, J. Chen, X. Zhu, G. Hu, P. Peng, Z. Zheng, and H. Zhang, Sci. Rep. **7**, 42357 (2017).

[28] L. Chen, C. Zhang, L. Li, H. Wu, X. Wang, S. Yan, Y. Shi, and M. Xiao, J. Phys. Chem. C **121**, 12972 (2017).

[29] W. Chen, K. Li, Y. Wang, X. Feng, Z. Liao, Q. Su, X. Lin, and Z. He, J. Phys. Chem. Lett. **8**, 591 (2017).

[30] Y. Yang, J. Gao, Z. Zhang, S. Xiao, H.-H. Xie, Z.-B. Sun, J.-H. Wang, C.-H. Zhou, Y.-W. Wang, X.-Y. Guo, P. K. Chu, and X.-F. Yu, Adv. Mater. **28**, 8937 (2016).

[31] M. Batmunkh, M. Bat-Erdene, and J. G. Shapter, Adv. Energy Mater. **1701832**, 1701832 (2017).

[32] L. L. Li, D. Moldovan, W. Xu, and F. M. Peeters, Phys. Rev. B **96**, 155425 (2017).

[33] M. S. Devadas, T. Devkota, P. Johns, Z. Li, S. S. Lo, K. Yu, L. Huang, and G. V. Hartland, Nanotechnology **26**, 354001 (2015).

[34] A. Arbouet, D. Christofilos, N. Del Fatti, F. Vall?e, J. R. Huntzinger, L. Arnaud, P. Billaud, and M. Broyer, Phys. Rev. Lett. **93**, 127401 (2004).

[35] T. Devkota, M. S. Devadas, A. Brown, J. Talghader, and G. V. Hartland, Appl. Opt. **55**, 796 (2016).

[36] A. N. Rudenko, S. Yuan, and M. I. Katsnelson, Phys. Rev. B **93**, 199906(E) (2016).

[37] T. Yamamoto, T. Noguchi, and K. Watanabe, Phys. Rev. B **74**, 121409 (2006).

[38] H. Abdelsalam, M. H. Talaat, I. Lukyanchuk, M. E. Portnoi, and V. A. Saroka, J. Appl. Phys. **120**, 014304 (2016).

[39] V. A. Saroka, K. G. Batrakov, and L. A. Chernozatonskii, Phys. Solid State **56**, 2135 (2014).

[40] V. A. Saroka, K. G. Batrakov, V. A. Demin, and L. A. Chernozatonskii, J. Phys.: Condens. Matter **27**, 145305 (2015).

[41] V. A. Saroka and K. G. Batrakov, Russ. Phys. J. **59**, 633 (2016).

[42] X. Peng, A. Copple, and Q. Wei, J. Appl. Phys. **116**, 144301 (2014).

[43] D. J. DiMaria, E. Cartier, and D. Arnold, J. Appl. Phys. **73**, 3367 (1993).

[44] E. V. Castro, K. S. Novoselov, S. V. Morozov, N. M. R. Peres, J. M. B. L. dos Santos, J. Nilsson, F. Guinea, A. K. Geim, and A. H. C. Neto, Phys. Rev. Lett. **99**, 216802 (2007).
[45] S. B. Lu, L. L. Miao, Z. N. Guo, X. Qi, C. J. Zhao, H. Zhang, S. C. Wen, D. Y. Tang, and D. Y. Fan, Opt. Express **23**, 11183 (2015).
[46] M.-F. Lin and F.-L. Shyu, J. Phys. Soc. Jpn. **69**, 3529 (2000).
[47] K.-I. Sasaki, K. Kato, Y. Tokura, K. Oguri, and T. Sogawa, Phys. Rev. B **84**, 085458 (2011).
[48] V. A. Saroka, M. V. Shuba, and M. E. Portnoi, Phys. Rev. B **95**, 155438 (2017).
[49] H. Hsu and L. E. Reichl, Phys. Rev. B **76**, 045418 (2007).
[50] H. Abdelsalam, H. Elhaes, and M. A. Ibrahim, Chem. Phys. Lett. **695**, 138 (2018).
[51] D. Mombrú, M. Romero, R. Faccio, and Á. W. Mombrú, J. Phys. Chem. C **121**, 16576 (2017).
[52] J. S. de Sousa, M. A. Lino, D. R. da Costa, A. Chaves, J. M. Pereira, Jr., and G. A. Farias, Phys. Rev. B **96**, 035122 (2017).
[53] L. Shao, H. Ye, Y. Wu, D. Yinxiao, P. Ding, F. Zeng, and Q. Yuan, Mater. Res. Express **3**, 025013 (2016).
[54] X. Wang, A. M. Jones, K. L. Seyler, V. Tran, Y. Jian, H. Zhao, H. Wang, L. Yang, X. Xu, and F. Xia, Nat. Nanotechnol **10**, 517 (2015).